J MATER SCI 41 (2006) 2097–2112

Effect of nitrogen addition on the microstructure and mechanical behavior of 317L and 904L austenitic stainless steel welds

DEEPASHRI D. NAGE, V. S. RAJA*
Corrosion Science and Engineering, Indian Institute of Technology, Bombay, Mumbai, 400 076, India
E-mail: vsraja@met.iitb.ac.in

R. RAMAN
Department of Metallurgical Engineering and Materials Science, Indian Institute of Technology, Bombay, Mumbai, 400 076, India

A systematic study of the effect of nitrogen addition on the microstructure and mechanical behavior of two different austenitic stainless steel welds, namely, 317L and 904L was carried out. For this, nitrogen content of the welds was altered by introducing different proportions of nitrogen gas into the argon shielding gas during welding. Nitrogen addition to 317L weld changed solidification mode from primary ferrite to primary austenite. As 904L weld solidify by primary austenitic mode, no change in the solidification mode was found with N addition. The results showed that, with rise in nitrogen content of the welds, various mechanical properties like ultimate tensile strength and ductility had improved significantly and that the welds prepared with 1 vol% N_2 in the shielding gas indeed failed in the base alloy making the weld stronger than the parent metal. It was noticed that the effect of N towards improving the mechanical properties 904L weld was higher than that found in the case of 317L weld.

1. Introduction

Austenitic stainless steels are widely used in various industries as structural material, as they possess a combination of properties like high strength and ductility, good formability and versatile fabricability. Nitrogen as an alloying element is found to offer several attractive properties to austenitic stainless steels. With innovations in melting technology, nitrogen (an austenite stabilizer) addition as an alloying element has become one of the least expensive ways to compensate for Ni in austenitic stainless steels [1]. There exists a lot of literature on the effect of nitrogen addition on the mechanical and corrosion properties of the wrought alloys [2–6]. Nitrogen can substitute carbon, as both of these form interstitial solid solution strengthening in the austenitic stainless steels. Nitrogen enhances the yield strength of the alloy, while retaining its ductility [1, 7, 8]. Moreover, precipitation kinetics of intermetallic compound formation in stainless steels is found be suppressed in stainless steels, when nitrogen is present at lower levels [9], though it can form nitrides, if its concentration exceeds certain level. Formation of nitride can adversely affect corrosion and mechanical properties of the alloy. Small amounts of nitrogen in austenitic stainless steels affect delta ferrite-austenite duplex microstructure, reducing the δ ferrite. This directly affect their mechanical properties and corrosion resistance [10].

In contrast to wrought alloys, welds have received lesser attention with regard to understanding the effect of nitrogen on various properties described above. A few authors have studied the effect of nitrogen on the localized corrosion behavior, such as pitting corrosion [11–15] and stress corrosion cracking [11–19] in a variety of environments. In particular, role of aging on the corrosion [20] as well as mechanical properties of welds have been studied by a few [21, 22]. On aging, the delta ferrite in the welds transforms to brittle phases such as sigma, chi etc. On prolonged aging, spherodisation of sigma occurs and homogeneity is attained. Thus, depending on aging,

*Author to whom all correspondence should be addressed.
0022-2461
DOI: 10.1007/s10853-006-3150-5

TABLE I Chemical composition (wt%) of 316L base alloy and 317L and 904L filler wires

	Elements									
Alloy	C	Cr	Ni	Mo	Si	Mn	S	P	Cu	N
316L	0.025	17.13	11.58	2.61	0.49	1.52	0.010	0.026	–	<0.010
317L	0.020	18.69	13.57	3.21	0.39	1.61	0.011	0.025	0.75	0.031
904L	0.010	19.95	25.00	4.35	0.37	1.89	0.001	0.013	1.39	0.037

various mechanical properties like ductility and strength changes. Notably, no significant work exists on the effect of delta ferrite and nitrogen on delta ferrite of as-welded alloys on their mechanical properties. This becomes relevant as most of the austenitic stainless steel welds are produced, with proper choice of consumables and welding parameters, avoiding fully austenitic mode of solidification. This is desirable in order to avoid solidification cracking [23, 24]. Unfortunately, due to limited time available during weld cooling, complete solid state transformation of ferrite to austenite is not possible leading to corrosion and mechanical problems during service. Addition of nitrogen during welding can affect not only the composition of the weld but also the kinetics of solid-state transformation characteristics of delta ferrite. This is expected to help in obtaining weld with low residual delta ferrite content without, at the same time, encouraging solidification cracking incidences. Extensive work in this direction has been undertaken in our laboratory [11–13, 16–18, 25]. The present study concerns with the effect of nitrogen on the mechanical properties of austenitic stainless steel welds. Two different filler wires namely, 317L—which solidifies by primary ferritic mode and 904L—which solidifies by primary austenitic mode, were chosen in the present study. In 904L weld, nitrogen affects only its composition and it does not influence the solidification mode, while in 317L weld, it affects both the solidification mode as well as the composition of the weld. Thus, the effect of nitrogen addition towards both these aspects can be understood by examining both these welds. The mechanical properties are related to microstructure of the weld and the solidification behavior. These aspects have been examined in the present study.

2. Experimental

316L sheets of 200 mm length, 100 mm width and 3.15 mm thick and filler wires of 317L and 904L having 3.2 mm diameter were used in the present study. The nominal chemical compositions of the base alloy and filler wires are given in the Table I. 'U' edge preparation was made at the center, along the length of the plate. Sectional view of this U-groove, giving various dimensions is shown in Fig. 1. U edge preparation over commonly used V edge was preferred as the former gave rise to lower weld dilution (>50%) than the latter (90%) under the present welding conditions. The U-groove dimensions were such that filler wire fitted very well in it. Welding was carried out using an automatic Transarc 500 (Fronius) tungsten

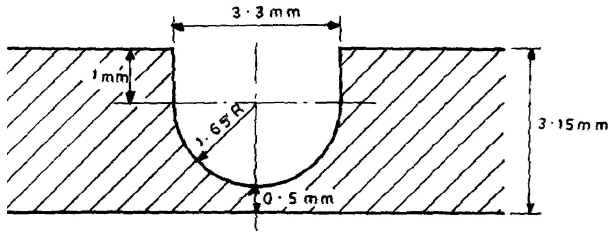

Figure 1 Dimension of U groove made on the stainless steel plate used for welding.

inert gas (TIG) welding machine. Ar gas at a flow rate of 8 l/min was used as a shielding gas. Nitrogen was also introduced in the Ar shielding gas. For this, the nitrogen was mixed with Ar in a specially designed mixing chamber, after it was sent through a rotameter to fix its levels in the shielding gas. The volume percentages of nitrogen used were 0, 0.5 and 1 of Ar shielding gas. Actually, in this study, the welds were produced even with 3 vol% N_2 in the shielding gas. As these welds were found to be porous, the study was restricted to welds prepared with nitrogen up to 1 vol% in the shielding gas. The welding parameters like the welding current and welding speed were standardized with many welding trials. The optimized weld parameters are given below. A welding speed of 4.3 mm/s was employed. The heat input used for welding was less than 0.3 kJ/mm. The gap between the non-consumable tungsten electrode tip and the top surface of the base plate was maintained to 4.5 mm. The welding currents optimized for 317L and 904L welds were 145 and 160 A respectively for the welds produced without nitrogen in the shielding gas. Upon introducing nitrogen in the shielding gas, the current values were reduced to 140 and 155 A for 317L and 904L welds respectively in the shielding gas. This is because nitrogen leads to higher penetration [26, 27]. The increased penetration is a result of Marangoni effect [10, 25]. The currents were adjusted so as to ensure reasonably similar dilution levels in all the welds. This has been done to ensure that the effect of nitrogen, which is the main theme of our work [16–18] is brought out reasonably clearly.

The Ferrite Number (FN) of the welds was measured by means of a calibrated Fischer Fe-8 ferritoscope along the length of weld. The average of 8–10 readings is given as the FN of the weld. The nitrogen content of the weld was analyzed from the chips of weld fusion zones by LECO test. The percentage dilution (%D) of the welds is calculated as below. The details of various abbreviations

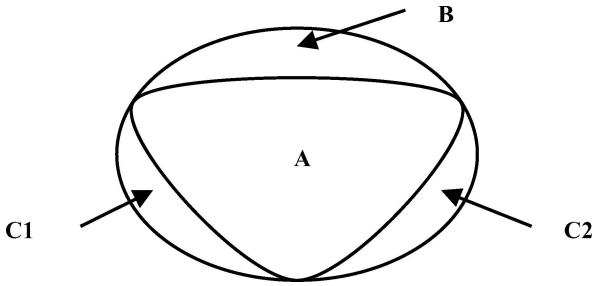

Figure 2 Schematic of transverse cross section of weld sherving various zones used for calculating percentage dilution.

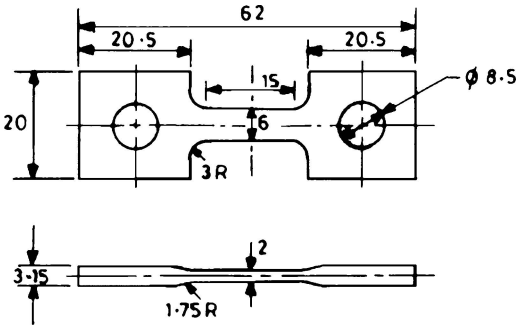

Figure 3 Dimension of tensile specimen used for the mechanical tests.

used in the following equation are delineated in Fig. 2.

$$\%D = \frac{(C_1 + C_2)}{(A + B + C_1 + C_2)} \times 100 \qquad (1)$$

where, A = Area of the U groove, B = Area of reinforcement of the weld, C1 and C2 = Area of diluted regions of the weld nugget.

%Dilution was calculated by taking a short transverse section of the weld and subjecting it to polishing, etching and then, projecting over profile projector to measure the nugget area. The initial area of the U groove A, is known. Therefore, (C1 + C2) can be easily found by deducting A + B from the measured area. Substituting in the above equations,% dilution can be obtained.

Cooling curves of the welds were obtained using the following setup. For this, 1 mm diameter and 1.5 mm deep hole was drilled on the filler wire used and a through hole at the centre of the U groove of the base plate. Filler wire was kept over the groove with the hole in it facing the hole of the base plate. A Pt/Pt-13%Rh thermocouple wire was inserted into the filler wire through the base plate. This enabled smooth passage of the welding electrode over the filler wire, while thermocouple was placed in the filler wire. The output of the thermocouple was recorded using a X-Y recorder. Such an arrangement enabled to obtain complete cooling curves without interruption. For microstructural studies, various sections of the weld fusion zones were cut, polished to mirror finish and color etched using modified Beraha's reagent [28, 29]. These samples were then observed over a Riechert MeFe3 microscope. X-ray diffraction (XRD) studies were carried out on the weldments in the range of 20 to 70° glancing angles at a scan rate of 1°/min, using Philips PW 1820 diffractometer with Cu K_α radiation.

Hardness measurements were carried out using Brinell hardness tester with 32.5 kg load. Flat pin loaded tensile specimens of 62 mm length were fabricated from transverse welds of 317L and 904L with different nitrogen contents. The dimension of the tensile specimen used in the study is shown in Fig. 3. The gauge length of the sample consisted of sections of weld fusion zone (FZ), heat affected zone (HAZ) and base alloy. The weld fusion zone in the gauge lay in such a way that weld transverse direction became parallel to the load axis and also lies at the center of the gauge section. Tensile tests were carried out using a 9 ton gear driven tensile testing machine. The tests were carried out at a strain rate of 2.2×10^{-6} s^{-1}. Various mechanical properties like ultimate tensile strength (UTS), % elongation (%e), % reduction in area (%RA) were reported. Apart from the above mentioned properties, %e of the weld fusion zone (FZ), failure location and the time-to-failure were also reported. The %e FZ was calculated as follows. The width of the FZ before the test was determined by etching the

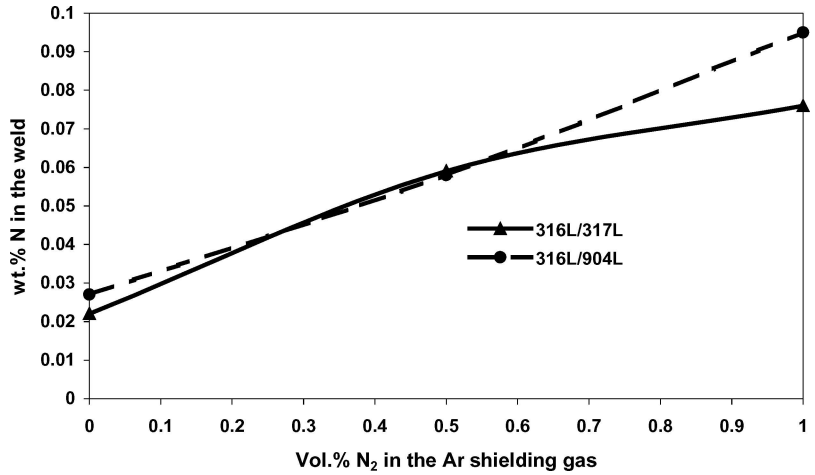

Figure 4 Effect of nitrogen in the shielding gas on the wt% N in the weld.

gauge of the specimen before tensile test. The width of the FZ upon elongation after test is quite visible due to straining effect. The difference of the latter and the former gives %e of the FZ. The fracture surfaces were observed using a Cambridge S-90 scanning electron microscope (SEM) at an operating voltage of 25 kV. Energy dispersive analysis by X-rays (EDAX) was also carried out along the dendrite and the interdendritic regions of the various welds.

3. Results and discussion

3.1. Phase and microstructural analysis

The variation of nitrogen content of the weld with nitrogen in the shielding gas is shown in Fig. 4. The figure shows that the wt% nitrogen in both 317L and 904L welds increased as the nitrogen in the shielding gas was increased. Such a rise in nitrogen content of the weld is in agreement with the work done by Okagawa *et al.* [10] and Lundin *et al.* [30]. It should be noted that welds prepared even without nitrogen in the shielding gas showed presence of nitrogen. This is because of the fact that the filler wires contained nitrogen. The reported values of welds are however, lower than that of 317L and 904L filler wire due to dilution of the weld by the base alloy, 316L which had very low nitrogen (<0.001 wt%) content. It should also be remembered that while welding nitrogen containing stainless steels, it is necessary that sufficient partial pressure of nitrogen is present or else there will be loss of nitrogen from the weld to the arc.

It is a noteworthy fact that between 904L welds and 317L welds, the former absorbs more nitrogen than the latter especially at high nitrogen levels in the shielding gas. This could possibly be due to the difference in the content of the alloying elements between the two welds. Cr is found to enhance nitrogen uptake of the welds in Fe-Cr and Fe-Ni alloys [26], as the presence of Cr increases the solubility of nitrogen in stainless steels [7]. Although, nickel has a slight negative influence on the solubility of nitrogen in liquid stainless steel [7], it has been reported by Kuwana and Kokawa [27] that at high heat inputs Ni actually promotes nitrogen pick up. Though high heat input is generally unfavorable for nitrogen pickup of the weld [31], high Ni content of 904L weld seems to have promoted high nitrogen solubility. Thus, the observation as seen in Fig. 4 should be attributable to difference in alloying elements content and characteristic behavior of absorption phenomena under electric arc.

The X-ray diffractograms obtained for both the systems with various nitrogen contents of the shielding gas are shown in Figs 5a and b for 317L and 904L welds respectively. The patterns in both the cases can be indexed satisfactorily for an austenite phase. However, small amount of δ ferrite was noticed, in the case of 317L weld obtained with 0 vol% N_2 in the shielding gas, as revealed by the presence of (110) peak. Upon nitrogen addition to this system, this peak corresponding to δ ferrite was found to have disappeared. The ferritoscope and optical microscope studies further confirmed the X-ray diffraction data. It showed a Ferrite Number (FN) of 8. The micrograph shows (Fig. 6a) retained ferrite in the core of the dendrites having vermicular morphology. The volume fraction of delta ferrite was also determined by quantitative metallography and found to be around 8 vol%. As the nitrogen con-

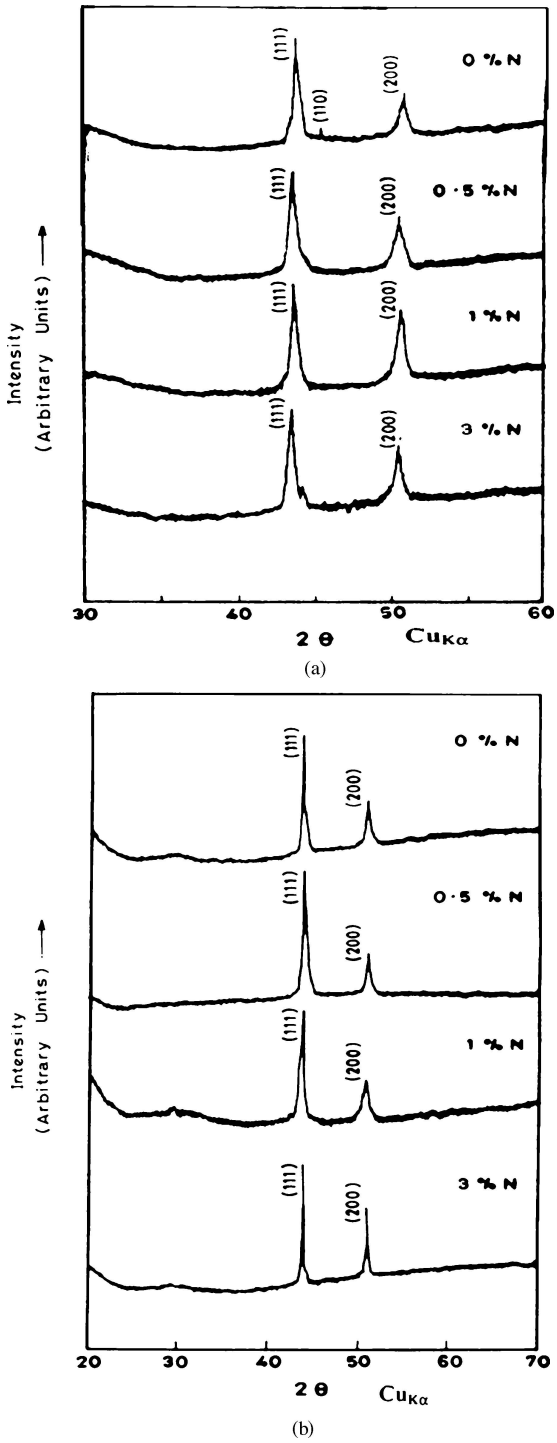

Figure 5 X-ray diffraction patterns of (a) 317L and (b) 904L welds with different nitrogen contents. The peaks (111) and (200) correspond to austenite and (110) correspond to ferrite phase. It is clear from 317L patterns that with nitrogen addition the (110) peak disappeared. This is because the ferrite transforms to austenite completely with nitrogen addition.

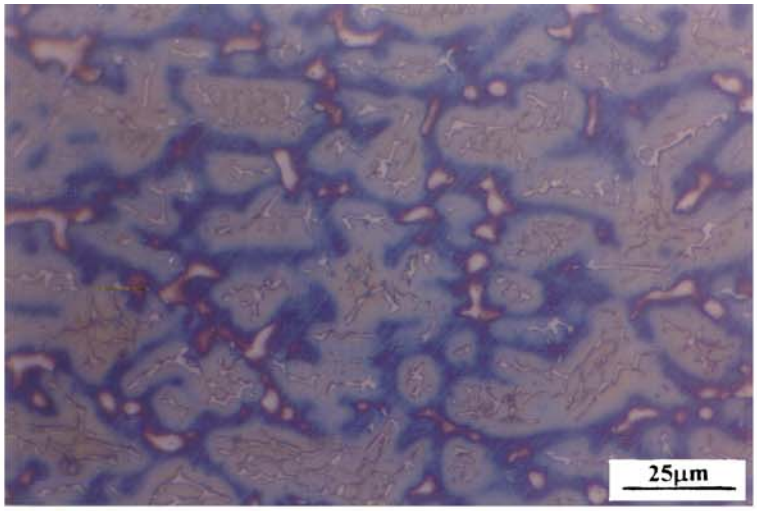

(a)

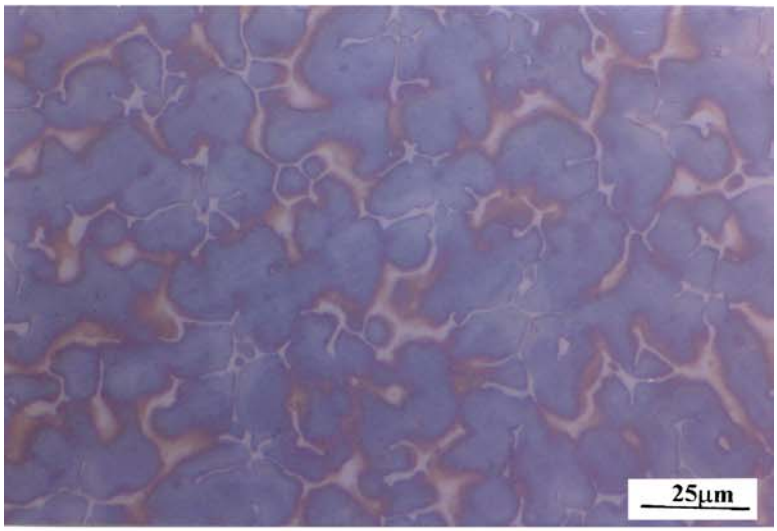

(b)

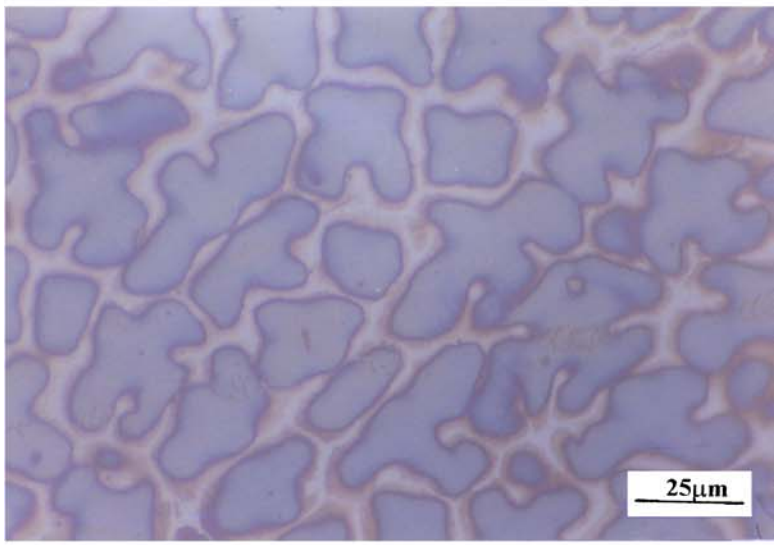

(c)

Figure 6 Optical micrographs of 317L welds prepared with (a) 0 vol% N_2, showing vermicular delta ferrite in the dark austenite dendrites (b) 0.5 vol% N_2 and (c) 1 vol% N_2 in the Ar shielding gas. The apparent interdendritic network of b and c micrographs are due to secondary austenite.

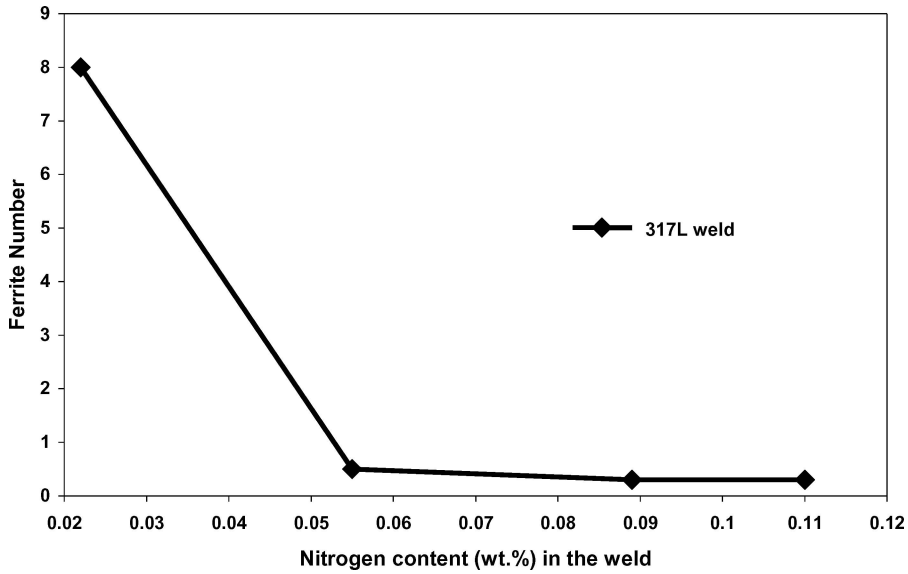

Figure 7 Effect of nitrogen additions on the Ferrite Number (FN) of 317L welds.

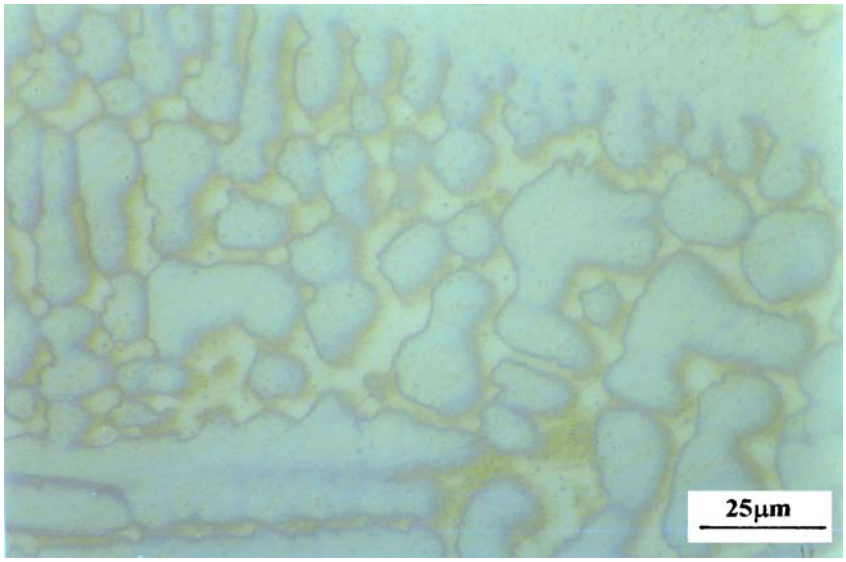

Figure 8 Typical optical micrographs of 904L welds prepared with 0 vol% N_2 in the Ar shielding gas. The contrast in dendrite and interdendritic austenite is due to Ni rich and Ni lean phases respectively.

tent of the weld was increased, both ferritoscope (Fig. 7) and optical micrographs (Fig. 6b, c) did not reveal the presence of delta ferrite supporting the X-ray diffraction studies.

A few optical micrographs of 317L and 904L welds in black and white contrast are shown in Figs 6a, b, c and 8. Figures illustrate various types of microstructures obtained in these welds. The original color micrographs showed diotinet variations in color contrast depending upon the chemical composition of the phases. According to the literature, Ni rich phases exhibit color contrast varying from blue to green and Cr rich phases exhibiting color contrast varying from reddish to yellow [28, 29]. The color variation is due to differences in the thickness of the sulphide film formed over the underlying substrate. Higher the thickness darker is the coloration, i.e., blue to green. Hence, delta ferrite appears with white contrast, while the austenite with blue contrast. In black and white contrast three distinct regions are seen in micrograph Fig. 6a of welds prepared with 0 vol % N_2 in the Ar shielding gas. Ni-rich and Cr lean regions representing austenite phase appear black. Ni-lean and Cr-rich regions representing δ-ferrite phase appear white. An inbetween gray shade correspond to austenite phase. Note the vermicular morphology of the δ-ferrite phase within the austenite phase. The microstructure obtained corresponds to ferrito-austenitic mode of solidification. Comparing the Figs 6a, b and c, it can be said that nitrogen addition completely suppresses primary delta ferrite phase in the dendrite cores even at 0.5 vol% N_2 in the shielding gas and further addition does not bring out any significant changes in the microstructure of the weld. As

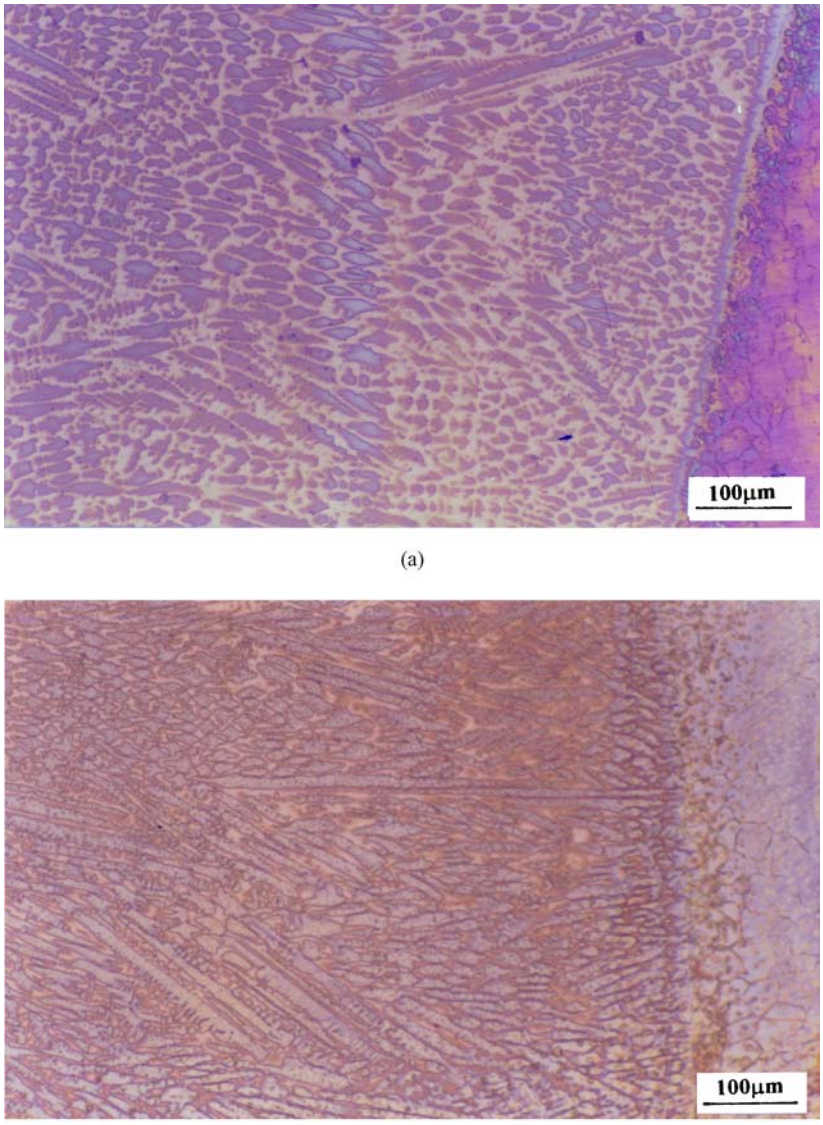

Figure 9 Comparison of 904L welds (a) with and (b) without nitrogen. The volume percentage of interdendritic phase seems to have increased with nitrogen additions.

seen from Figs 6a, b and c, addition of nitrogen to the welds has resulted in the cores of the dendrites becoming darker and the interdendritic regions lighter in color (i.e., austenite (Ni rich) nucleates first and the Cr rich austenite at the interdendritic regions). This indicates that addition of nitrogen has changed the solidification mode from primary δ to primary γ. This is also in agreement with XRD and ferritoscope data as discussed earlier. From color contrast, it can be said that 904L welds have dendrites (darker in color), which are Ni-rich austenite, and interdendritic (lighter in color) regions, which are Cr rich austenite.

The microstructure of welds depends on various factors like the consumables composition and welding parameters. These parameters include welding current, welding speed, thereby heat input, which directly influence the dilution content of the weld. From dilution, we can also judge the relative cooling rates of different welds, provided the weld-groove and filler wire dimensions remained the same. Based on cooling rates, extent of dilution and the volume fraction of the interdendritic phases vary. The amounts of dilution obtained for 317L welds are 47, 43 and 41% and for 904L are 63, 61 and 59% for welds with 0, 0.5 and 1 vol% N_2 in the shielding gas respectively. The welding current used for 904L was higher than 317L therefore %dilution was higher for 904L welds than 317L welds. When the filler wire and base metal compositions differ, the variation in dilution can alter the weld composition and so can influence the solidification mode. Also, for a given dilution, the addition of nitrogen is expected to promote more of primary austenite phase. Comparison of micrographs (Fig. 9a and b) shows that upon nitrogen addition, the volume fraction of interdendritic phase increased.

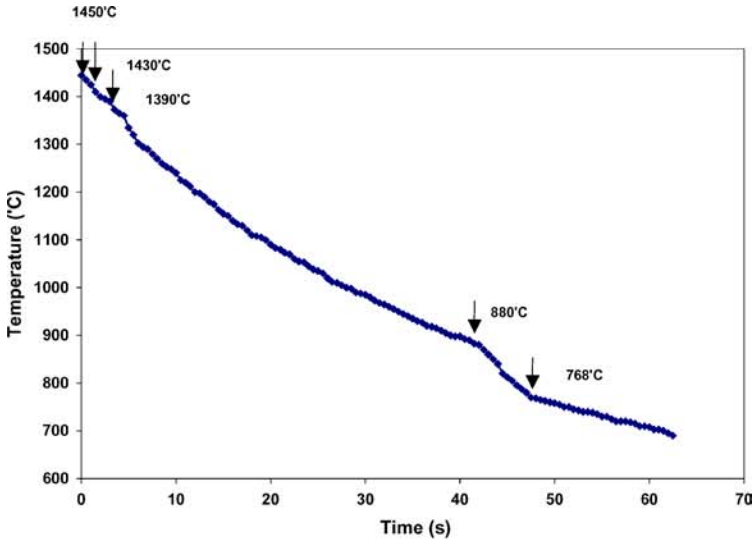

(a)

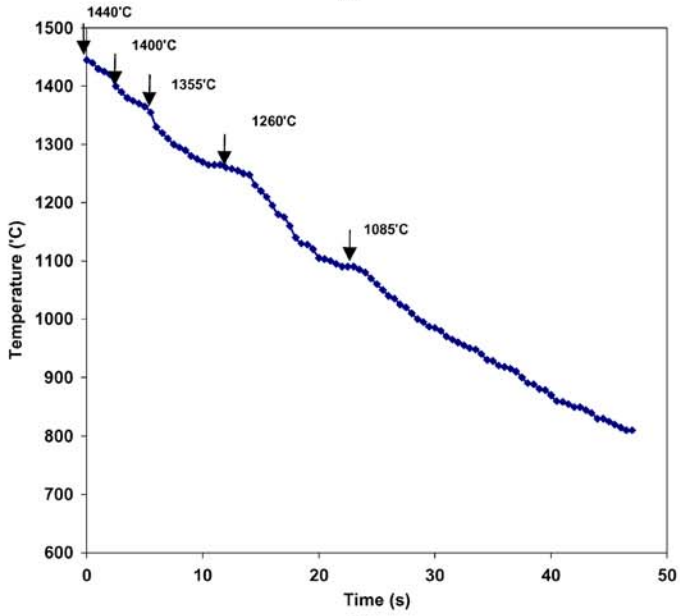

(b)

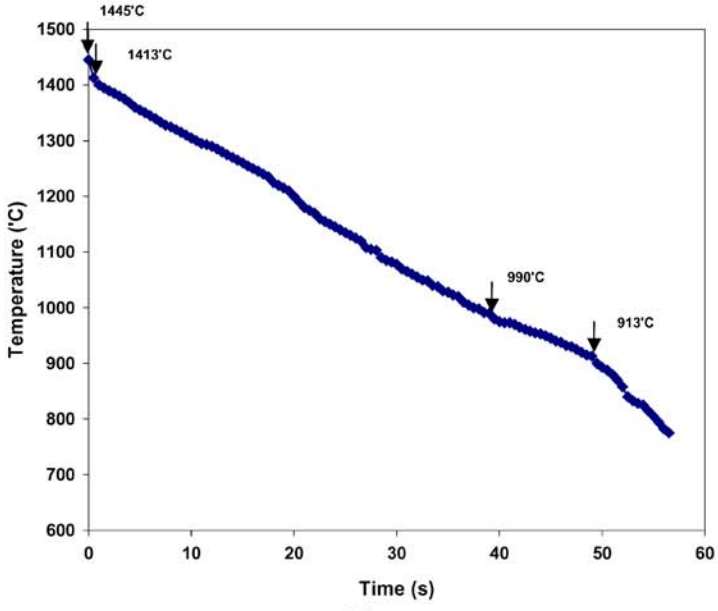

(c)

Figure 10 Cooling curves of 317L weld with (a) no nitrogen (b) 0.5 vol% nitrogen and (c) 1 vol% nitrogen in the Ar shielding gas. The arrows indicate various transition temperatures.

As the literature on the solidification behavior of the welds with respect to cooling curves is scanty, the present study obtained the cooling curves of 317L and 904L welds with and with out nitrogen additions to the shielding gas. Figs 10 and 11, show typical cooling curves of 317L and 904L welds respectively. The inflection points, where the slope of the cooling curves were found to change with time, were summarized in the Tables II and III for 317L and 904L welds respectively. The location of the inflection points seen visually were further confirmed through local derivatives of the curves (not shown in the figures).

TABLE II Various transition temperatures recorded during cooling of 317L welds with different nitrogen contents in the Ar shielding gas

vol% N_2	Transition temperatures (°C)				
0	1450	1430	1390	880	768
0.5	1440	1400	1355	1260	1085
1	1445	1413	990	913	–

In order to examine the possible phase transitions at these inflection points and correlate to X-ray diffraction, optical microscope and ferritoscope data,

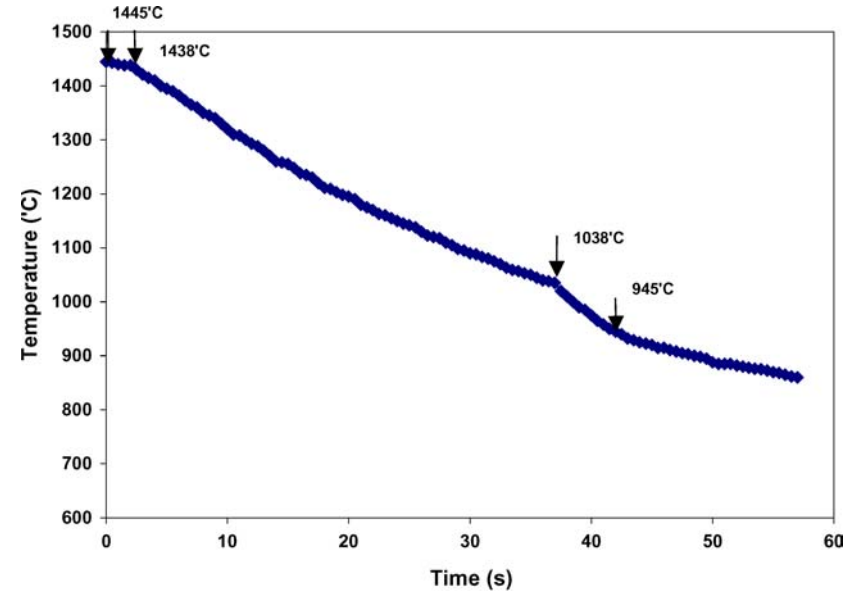

(a)

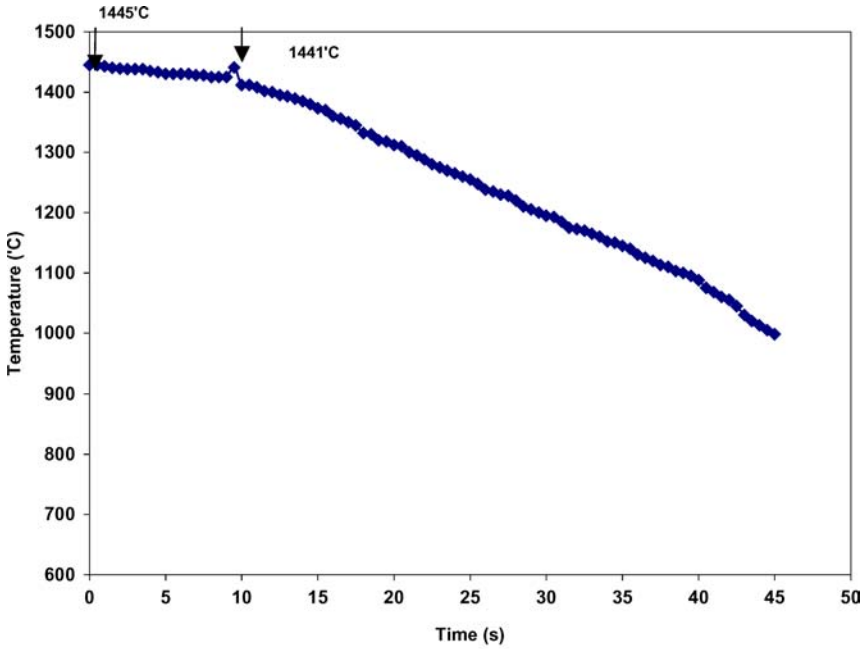

(b)

Figure 11 Cooling curves of 904L weld with (a) no nitrogen (b) 0.5 vol% and (c) 1 vol% nitrogen in the Ar shielding gas. in the Ar shielding gas. The arrows indicate various transition temperatures.

(*Continued on next page.*)

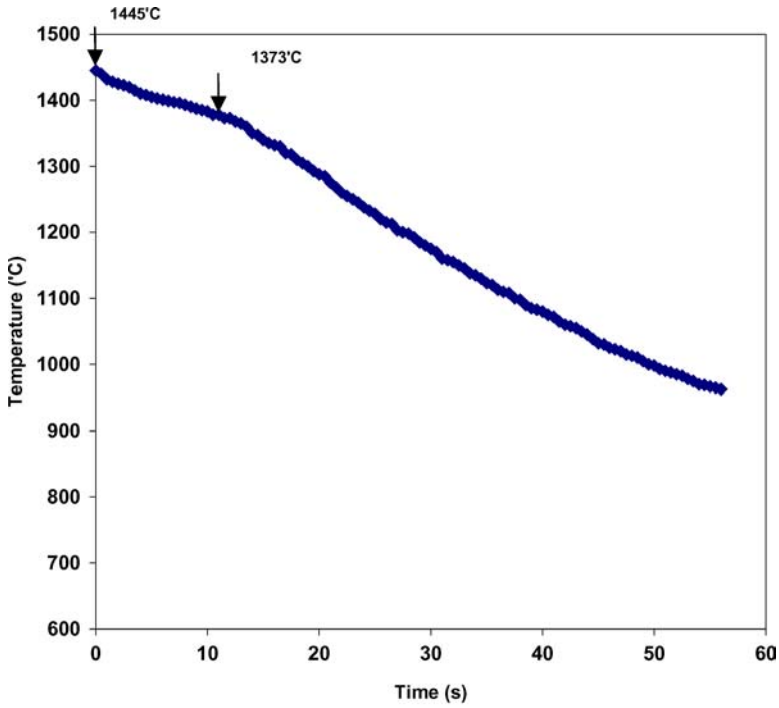

(c)

Figure 11 (*Continued*).

pseudo binary phase diagrams of 65Fe-*x*Ni-*y*Cr (Fig. 12 [32]) and 60Fe-*x*Ni-*y*Cr (Fig. 13 [33]) systems, whose Fe contents are close to that of 317L and 904L welds respectively, are considered for discussion. Location of the composition of the weld in pseudo binary diagram is fixed as follows. First, the Ni_{eq} values of welds with different nitrogen contents based on percentage dilution were determined. Second, the Ni content of the alloy of the phase diagram that gives rise to the above Ni_{eq} value of the weld was calculated. The following equation was used to obtain Ni equivalent of all the systems [34].

$$Ni_{eq} = Ni + 0.5Mn + 30C + 30N \qquad (2)$$

Based on various equivalents calculated for each of the weld, solidification lines for 317L and 904L welds were drawn in the diagrams. Thus, the vertical lines 1–5 correspond respectively to 316L base alloy, 317L filler wire, 317L weld with 0 vol% N_2 in the Ar shielding gas, 317L weld with 0.5 vol% N_2 in the Ar shielding gas and 317L weld with 1 vol% N_2 in the Ar shielding gas respectively. Similarly, the lines 1–4 of Fig. 13 correspond respectively to 904L filler wire, 904L weld with 0 vol% N_2 in the Ar shielding gas, 904L weld with 0.5 vol% N_2 in the Ar shielding gas

TABLE III Various transition temperatures recorded during cooling of 904L welds with different nitrogen contents in the Ar shielding gas

vol% N_2	Transition temperatures (°C)			
0	1445	1438	1038	945
0.5	1445	1441	–	–
1	1445	1373	–	–

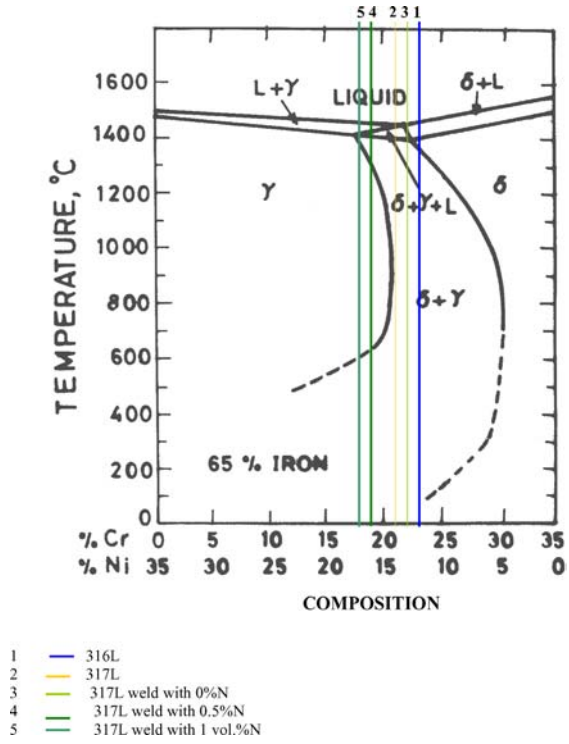

Figure 12 Pseudo-binary diagram of 65Fe-*x*Ni-*y*Cr system [32] is provided to illustrate possible phase transition occurring in 317L welds with varying nitrogen contents.

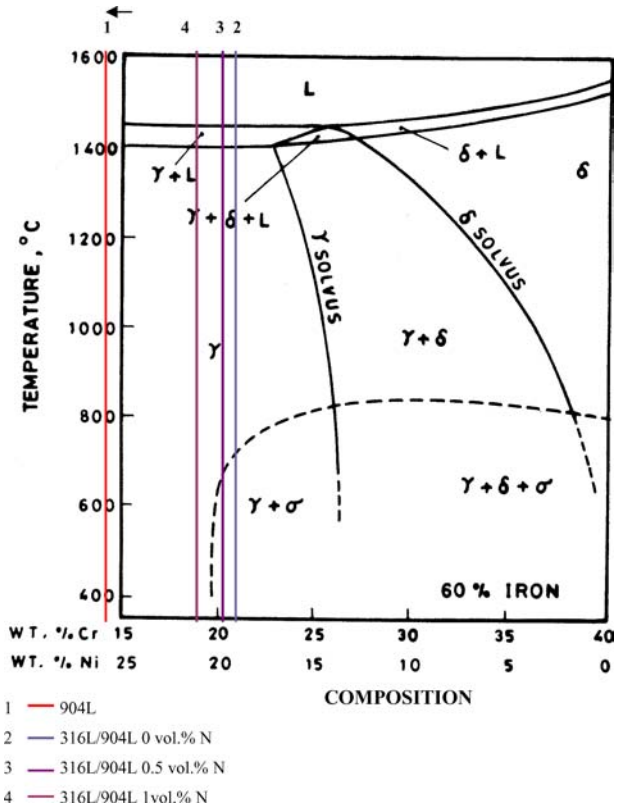

Figure 13 Pseudo-binary diagram of 50Fe-*x*Ni-*y*Cr system [33] is provided to illustrate possible phase transition occurring in 904L welds with varying nitrogen contents. Arrow indicates 904L is out of the range.

and 904L weld with 1 vol% N_2 in the Ar shielding gas respectively. Notably, 317L and 904L filler wires obtained by the above method show that they solidify by primary delta ferrite and primary austenitic modes of solidification respectively. This is in accordance with the suggestion by Suutala *et al*. [35] that weld metals with Cr_{eq}/Ni_{eq} ratios of 1.5 (317L) and 0.95 (904L) should solidify by primary delta ferrite and primary austenitic modes respectively. Further more, the present results of X-ray diffraction, optical microscope and ferritoscope techniques are in agreement with this. For this reason, finding an equivalent composition in the phase diagram for the purpose of understanding the solidification seems to be acceptable. Table II shows that 317L weld with no nitrogen exhibits four transitions in the temperature ranges (a) 1450–1430°C, (b) 1430–1390°C, (c) 1390–880°C and (d) 880–768°C. Looking at the pseudo-binary phase diagram the first transition should correspond to $L \rightarrow \delta + L$. This seems to be possible, as the solidification range measured and shown by the pseudo-binary diagram are narrow. The subsequent transition occurring between 1430–1390°C should correspond to the transition $L + \delta \rightarrow \delta + \gamma +$ L. This occurs over a broader range of temperatures than the first reaction, which is in agreement with the phase diagram. Below 1390°C the reaction $\delta + \gamma + L \rightarrow \delta + \gamma$ is expected to occur. From the Fig. 12, it appears that a value of 1400°C should have been obtained. This could possibly be attributed to requirement of some undercooling for liquid to solid state transformation, although some solid phases already exists. This is possible under welding conditions where cooling rates are quite rapid. The transition occurring between 880 and 768°C should correspond to the formation secondary austenite, γ', represented by the reaction $\delta \rightarrow \gamma'$. As described earlier, γ' is the product formed from a solid state transformation of δ ferrite. It is hard to distinguish how much of primary (in the cores of dendrites) and eutectic δ (in the interdendritic regions) transform into secondary austenite. The micrographs (Fig. 6a) however, show secondary austenite predominantly located at the interdendritic regions, indicating that eutectic δ is more favorable for transformation, but it is also possible that some amount of primary δ solidifying later will also transform into γ'. The solidification behavior of the 317L weld obtained with 0.5 vol% N_2 in the shielding gas seems to differ from the previous case. The corresponding micrograph (Fig. 6b) of this weld shows no δ ferrite nor does the XRD and ferritoscope data indicated the presence of δ in the weld. The microstructure shows primary γ in the dendrite cores, with the first transition occurring between 1440–1400°C attributable to $L \rightarrow \gamma + L$. The subsequent transition occurring between 1400–1355°C can be attributed to the transition, $L + \gamma \rightarrow \delta + \gamma + L$. Subsequently, $\delta + \gamma + L \rightarrow \delta + \gamma$ occurring at 1260°C. Below this temperature (1085°C) the reaction $\delta + \gamma \rightarrow \gamma + \gamma'$ is expected to occur as per the phase diagram. Notably the reaction, $\delta \rightarrow \gamma'$ of the previous system occurs at higher temperature in conformity with the phase diagram. With 1 vol% N_2 in the shielding gas, the 317L weld does not show the reaction ($\delta + \gamma + L \rightarrow \delta + \gamma$) exhibited by the weld, but shows a transition to be occurring between 990 and 913°C. The absence of the above reaction may be due to the fact that, the volume of the eutectic product is lesser than that of the previous weld and so no significant change in the cooling curve is anticipated. The fact that interdendritic regions resemble secondary austenite and a transition has been observed between 990–913°C, the eutectic product does form, which may transform to secondary austenite.

Comparing the Tables II and III making similar arguments as has been done in the case of 317L weld with nitrogen, which solidify by primary γ, the following reactions can be written for 904L welds, $L \rightarrow L + \gamma$ and further, $L + \gamma \rightarrow \gamma$. It is to be noted that the cooling curve of 904L weld obtained without nitrogen in the shielding gas somewhat resembles that of 317L weld obtained with 1 vol% N_2 in the shielding gas. When the nitrogen is added to 904L, the transitions occurring between 1038 and 945°C are not seen. This is possibly because of the fact that, nitrogen addition moves the Ni_{eq} towards higher value, enough to reduce the eutectic reaction and hence no significant transition from eutectic delta ferrite to austenite is possible. 904L is expected to solidify by primary austenitic mode, which is a stable phase even to a temperature of room temperature. The X-ray diffraction and ferritoscope data too supports for presence of only austenite phase.

TABLE IV Mechanical properties of various transverse welds

Material	Nitrogen content in the shielding gas (vol% N_2)	Nitrogen content in the weld (wt% N)	UTS (MPa)	%e	%e of weld fusion zone (FZ)	%RA	Failure location
316L Base alloy	–	<0.001	644	61	–	61	Gauge
317L Weld	0	0.022	604	32	32	38	Weld
	0.5	0.059	630	40	35	45	Weld
	1	0.076	652	41	39	51	Parent
904L Weld	0	0.027	578	25	23	40	Weld
	0.5	0.058	591	29	25	46	Weld
	1	0.095	656	43	49	54	Parent

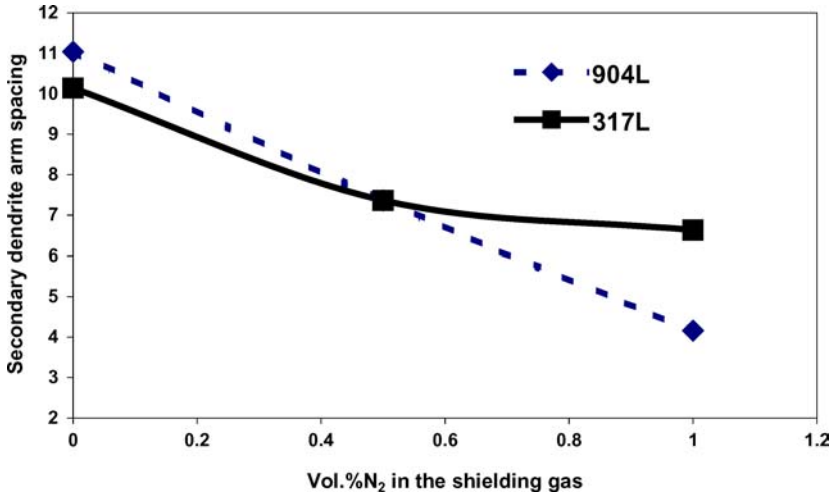

Figure 14 Effect of nitrogen on the secondary dendrite arm spacing (μm).

The spacing between the secondary dendrite arms can give idea about solidification kinetics. The variation in secondary dendrite arm spacing of the 317L and 904L welds without and with nitrogen in the Ar shielding gas was measured by a calibrated eyepiece over a micrometer objective. As the nitrogen content increased the secondary dendrite arm spacing was found to decrease (Fig. 14). The secondary dendrite arm spacing is a function of cooling rate and the mobility factor [36]. This mobility factor in turn depends on the surface tension and partition coefficient. This is ultimately dependent on the composition of the weld. As the heat input of all the welds was almost similar the cooling rates are assumed to not have varied much [31], thus the mobility factor seems to have influenced the secondary dendrite arm spacing. So, for the given system nitrogen is the only variable. Addition of nitrogen was found to decrease the secondary dendrite arm spacing. The details of the effect of nitrogen on the secondary dendrite spacing is given by the author elsewhere [37]. It should be noted that the extent of reduction in the secondary dendrite arm spacing was higher for 904L than in 317L welds. It would be interesting to carry out research in this particular direction of effect of nitrogen on the microstructure and morphology of welds.

3.2. Mechanical properties

Figs 15a and b show the load vs% elongation plots of 317L and 904L welds obtained during tensile tests. The plots with and without introducing nitrogen in the Ar shielding gas respectively are superimposed in one figure to illustrate the effect of nitrogen exclusively. The mechanical properties obtained from these plots, and failure location are summarized in Table IV. The data shows the following trend with respect to both the types of welds. Firstly, the strength and ductility of the weldment increases with a increase in nitrogen content of the weld. Secondly, the location of the failure shifts from the weld fusion zone to parent metal, when the N_2 content of the shielding gas becomes 1 vol%. It is worthwhile to examine how each of the welds responds to the N_2 addition. For this % elongation (%e) of the fusion zone (FZ) was measured in each of the cases.

The strength of 317L weld increases from 604 to 630 MPa, when the N_2 content of the shielding gas increased from 0 to 0.5 vol%. At 1 vol% the strength of the weld becomes 652 MPa. As this strength corresponds to that of the base metal, the failure occured in the base metal and away from heat-affected zone (HAZ). This indicated that the strength of the weld exceeded that of the base alloy. The hardness of the weld too increased (from 135 to

151 BHN) with increase in nitrogen contents in the welds. Notably, the ductility of the weld increased gradually with nitrogen addition to the weld. The highest value of 39% reported here might be lower than the true ductility of the weld fusion zone, because the parent metal failed before the weld fusion zone could elongate completely. 904L weld also exhibited a similar behavior though its strength levels were lower that of 317L welds, (compare strength levels of welds of 0, 0.5 vol% N_2). This is possible because 317L weld exhibits two phase structure (delta ferrite), while 904L has a single phase structure. The ductility of 904L welds too raised gradually with nitrogen additions. The highest values reported is 49%, which could be lower than the true ductility of the weld. This again is also because of the fact that the failure occurred in the parent metal and the weld fusion zone did not undergo complete elongation.

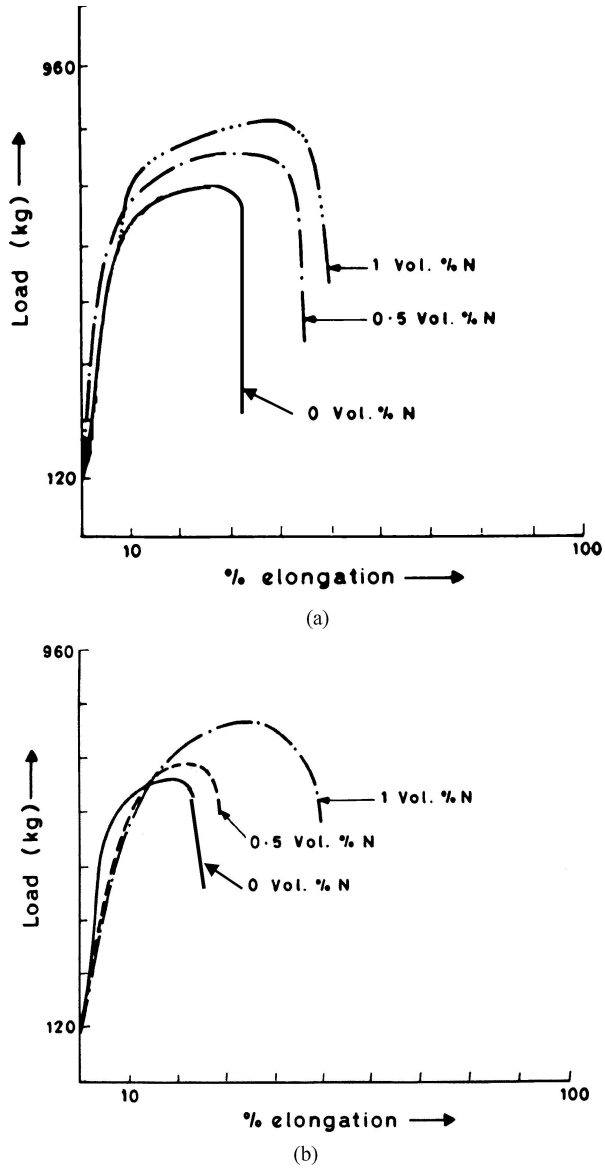

Figure 15 Load vs% elongation plots for (a) 317L and (b) 904L welds with different nitrogen contents in the shielding gas, tested at 2.2×10^{-6} s^{-1}. As the nitrogen content in the weld increases their strength and ductility increase.

There has not been a clear understanding on the role of delta ferrite and nitrogen on the mechanical properties of austenitic stainless steel welds. Literature on this subject is scanty. Reports are either directed towards the effect of thermal aging [21, 22, 38] or environment [19, 20] on the mechanical properties of the weld. Shaikh *et al.* reported that a decrease in delta ferrite content of the weld from 3 to 0 vol%, due to annealing at 1423 K, decreased the strength of the weld [22]. This result does not reflect just the effect of delta ferrite, as annealing also resulted in the formation of various phases, which also affect the mechanical property of the weld. Work by Baselack *et al.* [19] on the effect of delta ferrite on the stress corrosion cracking (SCC) behavior indicated that the maximum engineering stress of the weld exposed to boiling magnesium chloride decreased with a decrease in delta ferrite content. These authors brought down the delta ferrite content of the weld through the addition of nitrogen to the welds. However, in hydrochloric acid medium the SCC susceptibility of the weld seemed to decrease, when the delta ferrite was decreases from 12 to 2 FN. However, if the FN is increased from 12 to 24, again the SCC resistance increases [39]. Even Nage *et al.* have found a similar behavior in the case of 312 welds [13]. The mechanical strength both in air and in environment were found to increase with nitrogen addition and the consequent decrease in the delta ferrite.

The rise in the strength and ductility of 904L weld fusion zone with nitrogen addition indicated that nitrogen enhanced both the above properties of the weld in the absence of delta ferrite. Quite a few studies on the effect of nitrogen on the mechanical properties of wrought austenitic stainless steels have been reported [2–4, 6–8, 40, 41]. The extension of these mechanisms to welds might be difficult in view of the fact that the welds possess cast structures. However, the following factors could contributed towards the improved mechanical behavior of the welds. Firstly, nitrogen decreased the secondary dendrite arm spacing and secondly it strengthens the austenitic phase. The rise in the strength of the 317L despite a reduction in its delta ferrite content can be attributed to the overriding effect of nitrogen over delta ferrite, in the present system. The effect of reduction in secondary dendrite arm spacing and strengthening of austenite phase by nitrogen counters the loss in strength of the weld due to a reduction in delta ferrite content.

Close examination of the fractographs of the welds reveals interesting features illustrating the effect of nitrogen. Comparison of the fractographs of nitrogen containing 317L weld to that of nitrogen free weld indicates that nitrogen promotes localized deformation (Fig. 16a and b). Thus, fractograph of the weld with out nitrogen has large-size dimples compared with the smaller ones revealed in fractograph of the weld with nitrogen. The edge of the specimen in the fractograph (Fig. 17a) shows that the deformation in the weld with out nitrogen occurs preferen-

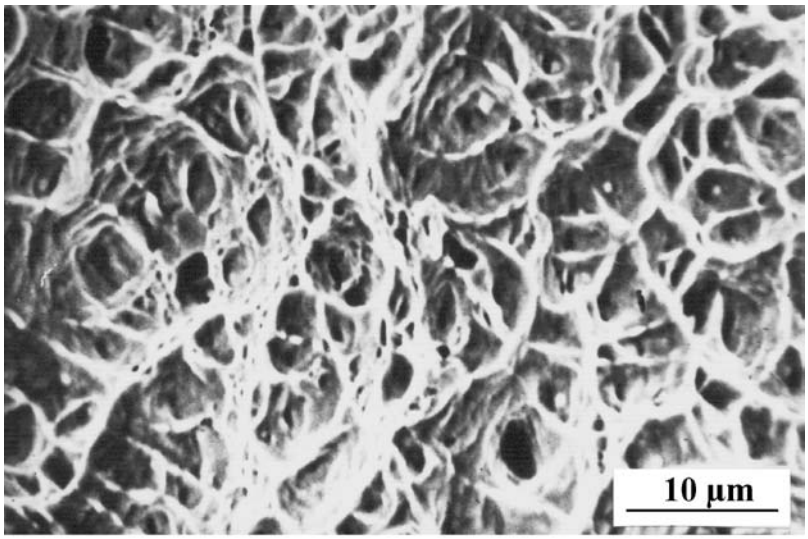

(a)

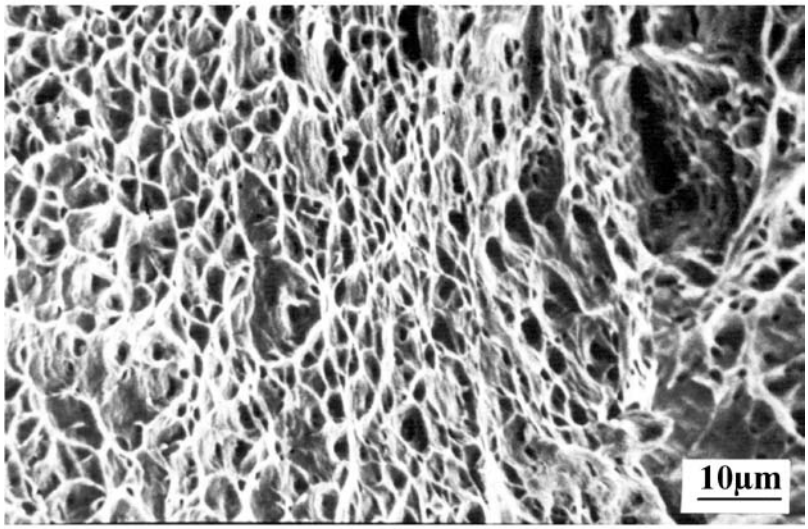

(b)

Figure 16 Fractographs of 317L weld prepared with (a) no nitrogen and (b) 0.5 vol% N_2 in the Ar shielding gas. Addition of nitrogen shows decrease in average dimple sizes indicating rise in ductility with rise in nitrogen contents.

tially along the interdendritic zones, which is less revealed in weld with higher nitrogen content (Fig. 17b). It was found that nitrogen minimized Si segregation along the interdendritic regions [17], which may not have allowed preferential deformation of this area (Table V). Though, the table reports value for 904L welds the explanation is implacable for 317L welds too. In this context, nitrogen affects the deformation behavior through minimizing segregation and even reduction in secondary dendrite arm spacing making the microstructure finer.

TABLE V EDAX results of 904L welds with 0.027 and 0.058 wt% N

	Weld with 0.027 wt% N		Weld with 0.058 wt% N	
Elements (wt%)	Dendrite	Interdendrite	Dendrite	Interdendrite
Cr	15.62	19.07	17.70	18.70
Ni	26.37	19.82	23.56	23.96
Si	0.12	1.35	0.60	0.94
Mo	3.14	4.57	4.03	4.45

4. Summary

Microstructure, X-ray diffraction data and ferritoscope data of 317L and 904L welds were correlated to solidification curves via pseudo-binary diagrams. There is a broad agreement among these data for all the welds with different nitrogen contents. As expected, both the welds were found to exhibit low strength and ductility in comparison with the parent metal, namely, 316L. However, nitrogen addition significantly improved their strength and ductility of the welds. About 1 vol% N_2 in the shielding

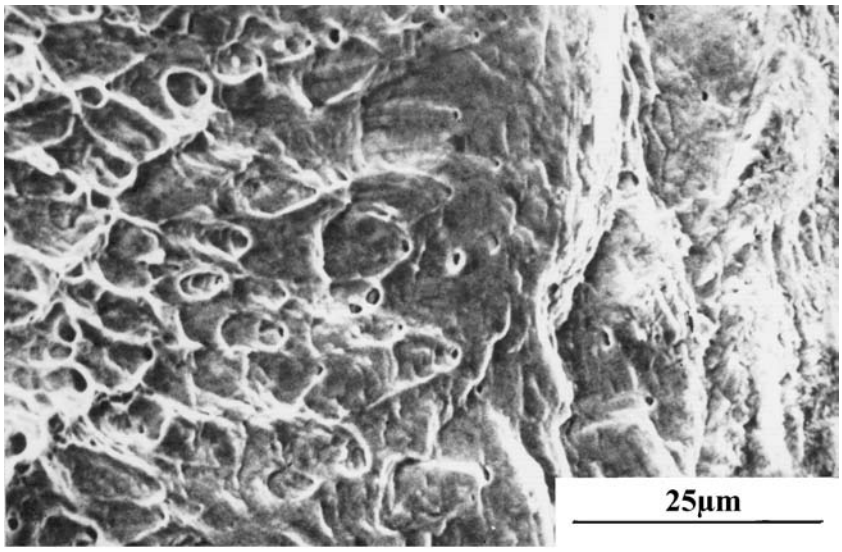

(a)

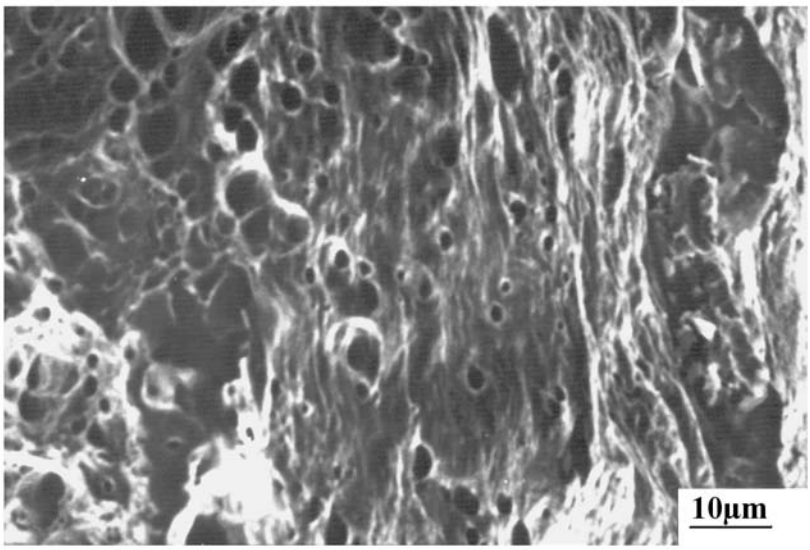

(b)

Figure 17 Edges of 317L welds prepared (a) without and (b) with 0.5 vol% N_2 in the shielding gas. Fractograph (a) show preferential crack growth which is not visible in case of welds prepared with nitrogen in the Ar shielding gas.

gas was adequate to raise the strength of the weld that the failure shifted from the weld fusion zone to the parent metal. Notably, nitrogen imparted higher strength to 904L weld than it did for 317L weld.

Acknowledgments

The authors acknowledge the financial support received from Department of Science and Technology, Government of India to carry out this work.

References

1. J. R. KEARNS and H. E. DEVERELL, *Mater. Perform.* **26**(6) (1987) 18.
2. V. G. GAVRILJUK, in Proceedings of 5th International Conference on High Nitrogen Steels, held in Espoo, Finland and Stockholm, Sweden, May 1998, edited by H. Hanninen, S. Hertz and J. Romu (Trans. Tech Publications Ltd., 1999) p. 3.
3. T. A. MOZHI, K. NISHIMOTO, B. E. WILDE and W. A. T. CLARKE, *Corrosion* **43** (1986) 197.
4. J. RAWERS and M. GRUJICIC, *J. Mater. Sci. and Engng. A* **A207** (1996) 188.
5. V. S. RAJA, in Proceedings of International Conference on Corrosion—CORCORN, Mumbai, (NACE India Section, 1997) p. 409.
6. M. O. SPEIDEL, in Proceedings of. International Conference on Stainless Steels, Chiba (ISIJ, 1991) p. l.
7. P. R. LEVEY and A. V. BENNEKOM, *Corrosion* **51** (1995) 911.
8. W. T. TSAI, B. REYNDERS, M. STRATMANN and H. J. GRABKE, *Corros. Sci.* **34** (1993) 1647.
9. T. OGAWA, S. AOKI, T. SAKAMOTO and T. ZAIZEN, *Weld. J.* **61** (1982) 139.
10. R. K. OKAGAWA, R. D. DIXON and D. L. OLSON, *ibid.* **62** (1983) 204s.
11. V. S. RAJA, *Corros. Reviews* **21**(1) (2003) 1.
12. V. S. RAJA, S. K. VARSHNEY, R. RAMAN and S. D. KULKARNI, *Corros. Sci.* **40** (1998) 1609.

13. D. D. NAGE, S. REDDY, R. RAMAN and V. S. RAJA, *Trans. Ind. Inst. Met.* **55** (2002) 447.
14. R. C. NEWMANN and T. SHAHRABI, *Corros. Sci.* **27** (1987) 827.
15. A. GARNER, *Corrosion* **35** (1979) 108.
16. D. D. NAGE, V. S. RAJA and R. RAMAN, in Proceedings of 13th Asian Pacific Corrosion Control Conference, Osaka, Nov. 2003, Paper No. 306.
17. D. D. NAGE, V. S. RAJA and R. RAMAN, Effect of nitrogen addition on the Stress corrosion cracking behavior of 904L welds in 288°C deaerated water, *Corros. Sci.* communicated.
18. D. D. NAGE, V. S. RAJA and R. RAMAN, in Proceedings of Corrosion Control and NDT, Nov. 2003, Paper No. 106.
19. BAESLACK III, W. A. DUQUETTE and W. F. SAVAGE, *Weld. J.* **58** (1979) 83s.
20. K. N. KRISHNAN and K. P. RAO, *Corrosion* **46** (1990) 734.
21. T. P. S. GILL, M. VIJAYALAKSMI, P. RODRIGUEZ and K. A. PADMANABHAN, *Met. Trans. A* **20A** (1989) 1115.
22. H. SHAIKH, T. V. VINOY and H. S. KHATAK, *Mater. Sci. Tech.* **14** (1998) 129.
23. F. C. HULL, *Weld. J.* **46** (1967) 399s.
24. C. P. D. LUNDIN, W. T. DELONG and D. F. SPOND, *ibid.* **54** (1975) 241s.
25. K. RAJASHEKHAR, in "Studies on the influence of nitrogen on weldability of stainless steels" (Ph. D. Thesis, I.I.T., Bombay, 1996).
26. T. KUWANA, H. KOKAWA and N. MURAMATSU, *Trans. Jpn Weld. Soc.* **20** (1989) 10.
27. T. KUWANA and H. KOKAWA, *ibid.* **19** (1988) 92.
28. P. LICHTENEGGER and R. BLOCH, *Prak. Metallographie* **12** (1975) 567.
29. G. F. VANDER VOORT, Color Etching in: Metallography and Microstructure, edited by K. Mills, J. R. Davis, J. D. Destefani, D. A. Dieterich, H. J. Frissel and D. M. Jenkins, 9th ed 9 (ASM Metals Park, Ohio, 1985), p. 139.
30. C. D. LUNDIN, C.-P. D. CHOU and C. J. SULLIVAN, *Weld. J.* **59** (1980) 226s.
31. A. GARNER, *Mater. Perform.* **21**(8) (1982) 9.
32. A. J. SEDRIKS, in "Corrosion of Stainless Steels" (John Wiley & sons, inc., New York, 1979) p. 50.
33. J. A. BROOKS and A. W. THOMPSON, *Int. Mater. Revi.* **36** (1991) 16.
34. W. T. DELONG, *Weld. J.* **53** (1974) 273s.
35. N. SUUTALA, T. TAKALO and T. MOISIO, *Met. Trans. A* **11A** (1988) 717.
36. G. OYSTEIN, in "Metallurgical Modeling of Welding" (The Institute of Materials, London, 1997) p. 265.
37. D. D. NAGE, V. S. RAJA and R. RAMAN, Effect of nitrogen on the secondary dendrite arm spacing, Communicated to Met. Trans. Under Revision.
38. R. G. BERGGREN, N. C. COLE, G. M. GOODWIN, J. O. STIEGLER, G. M. SLAUGHTER, G. J. GRAY and R. T. KING, *Weld. J.* **57** (1978) 167s.
39. W. A. BAESLACK III, D. J. DUQUETTE and W. J. SAVAGE, *Corrosion* **35** (1979) 45.
40. S. DEGALLIAX, J. I. DICKSON and J. FOCT, in Proceedings of 1st International Conference on High Nitrogen Steels, Lille, France, May 18–20, 1988, ed. J. Foct and A. Hendry (The Institute of Metals, London).
41. G. E. DIETER, in "Mechanical Metallurgy" (McGraw Hill Book Co., London, 1982) p. 189.

Received 29 January 2004
and accepted 13 April 2005